

Density Functional Theory Analysis of Molybdenum Isotope Fractionation[†]Colin L. Weeks,[‡] Ariel D. Anbar,^{§,||} Laura E. Wasylenki,[§] and Thomas G. Spiro^{*,‡}

Department of Chemistry, Princeton University, Princeton, New Jersey 08544, School of Earth & Space Exploration, Arizona State University, Tempe, Arizona 85287, and Department of Chemistry & Biochemistry, Arizona State University, Tempe, Arizona 85287

Received: June 4, 2007; In Final Form: July 13, 2007

Analytical studies have found an enrichment of the lighter Mo isotopes in oxic marine sediments compared to seawater, with isotope fractionation factors of -1.7 to -2.0 ‰ for $\Delta^{97/95}\text{Mo}_{\text{sediment-seawater}}$. These data place constraints on the possible identities of dissolved and adsorbed species because the equilibrium isotope fractionation depends on the energy differences between the isotopomers of the adsorbed species, minor dissolved species, and the dominant solution species, MoO_4^{2-} . Adsorption likely involves molybdic acid, whose structure is indicated by previous studies to be $\text{MoO}_3(\text{H}_2\text{O})_3$. Here we used DFT calculations of vibrational frequencies to determine the isotope fractionation factors versus MoO_4^{2-} . The results indicate that isotope equilibration of MoO_4^{2-} with $\text{MoO}_3(\text{H}_2\text{O})_3$, yielding $\Delta^{97/95}\text{Mo}_{\text{molybdic acid-molybdate}} = -1.33$ ‰, is most likely responsible for the isotope fractionation of Mo between oxic sediments and seawater. The difference between the calculated value of $\Delta^{97/95}\text{Mo}_{\text{molybdic acid-molybdate}}$ for $\text{MoO}_3(\text{H}_2\text{O})_3$ and the value observed in natural sediments and experiments is probably due to effects of solvation and adsorption onto the manganese oxyhydroxide surface.

Introduction

Molybdenum occurs in the oceans with a uniform concentration of $\sim 10^{-7}$ M. At this concentration and the typical ocean pH ~ 8 , Mo occurs in oxygenated seawater predominantly as the tetrahedral molybdate ion (MoO_4^{2-}). One of the quantitatively important ways that Mo is removed from seawater is by incorporation into ferromanganese oxide crusts and nodules that accumulate on the seafloor.^{1–3} Intriguingly, the isotopic composition of Mo differs between seawater and these sediments; the latter are enriched in the light Mo isotopes, with $\delta^{97/95}\text{Mo}$ of ferromanganese crusts lighter by -1.7 to -2.0 ‰.^{4,5} There is also evidence for the preferential adsorption of light Mo isotopes by manganese oxides in freshwater systems.⁶ Experiments on the Mo isotope fractionation during the adsorption of Mo from a MoO_4^{2-} solution onto manganese oxide have found a very similar isotope fractionation factor, $\Delta^{97/95}\text{Mo}_{\text{MnO}_x\text{-solution}} = -1.8$ ‰.⁷ Hence, the enrichment is thought to be due to an equilibrium isotope fractionation process between the Mo adsorbed to Fe/Mn oxyhydroxide surfaces and MoO_4^{2-} in solution. This fractionation is the basis of proposed geochemical applications of the Mo isotope system.^{4,5,8}

The mechanism of this isotope fractionation remains uncertain. Siebert et al. proposed that isotope fractionation occurs in solution between MoO_4^{2-} and molybdic acid (with the assumed structure $\text{Mo}(\text{OH})_6$), the latter being then preferentially adsorbed to ferromanganese oxide particle surfaces.⁵ Though molybdic acid would be only a trace species in seawater, it is in equilibrium with molybdate ion and would be selectively adsorbed onto sediments. Its adsorption would be the major mechanism by which Mo is taken up from oxic seawater.

The hypothesized mechanism is difficult to test directly in experiments, but it can be evaluated theoretically by calculating the expected isotope fractionation, from measured and/or computationally predicted vibrational frequencies for the proposed species. A critical factor in such evaluations is the assumed structure of molybdic acid, because the postulated isotope effect is driven by differences in the Mo coordination environment between the two species. A computational study by Tossell suggested that molybdic acid, instead of having the nominal structures $\text{MoO}_2(\text{OH})_2$ or $\text{Mo}(\text{OH})_6$, dissociates into MoO_3 and H_2O .⁹ Tossell further postulated that the MoO_3 species is adsorbed on the surface of the sediment and that the solution equilibrium between MoO_4^{2-} and MoO_3 is responsible for the experimentally observed isotope fractionation.

However, a recent Raman spectroscopic and density functional theory (DFT) study concluded that the most likely structure of molybdic acid in solution is $\text{MoO}_3(\text{H}_2\text{O})_3$,¹⁰ not MoO_3 . In the light of this result we have used DFT methods to calculate vibrational frequencies to determine the Mo isotope fractionation factor between MoO_4^{2-} and $\text{MoO}_3(\text{H}_2\text{O})_3$ as well as between MoO_4^{2-} and all the other possible structural isomers of molybdic acid. It was necessary to use calculated frequencies because most of the molybdic acid frequencies have not been measured experimentally.

Theoretical Calculations

Computations were performed with the Gaussian 03¹¹ program package. The calculations were carried out using the B3LYP^{12–14} DFT functional. The basis sets used were LANL2DZ ECP¹⁵ for Mo and 6-31+G(2df,p)^{16–20} for the H and O atoms. The calculations were performed using the B3LYP functional and the 6-31+G(2df,p) basis set for H and O atoms because previous work¹⁰ indicated that this gave the best balance between the accuracy of the frequency calculations and computational cost. Frequencies were calculated at the optimized geometries

[†] Part of the "Giacinto Scoles Festschrift".

* Corresponding author. Tel: +1-609-258-3907. Fax: +1-609-258-0348. E-mail: spiro@princeton.edu.

[‡] Princeton University.

[§] School of Earth & Space Exploration, Arizona State University.

^{||} Department of Chemistry & Biochemistry, Arizona State University.

for the ^{95}Mo and ^{97}Mo isotopomers of the following: MoO_4^{2-} , and of the possible molybdic acid structures $\text{MoO}(\text{OH})_4$, $\text{MoO}(\text{OH})_4(\text{H}_2\text{O})$, $\text{MoO}_2(\text{OH})_2$, $\text{MoO}_2(\text{OH})_2(\text{H}_2\text{O})$, $\text{MoO}_2(\text{OH})_2(\text{H}_2\text{O})_2$, MoO_3 , $\text{MoO}_3(\text{H}_2\text{O})$, $\text{MoO}_3(\text{H}_2\text{O})_2$, $\text{MoO}_3(\text{H}_2\text{O})_3$, and $\text{Mo}(\text{OH})_6$. Calculations were carried out in the gas phase and, for selected species, with a polarizable continuum model^{21–23} (PCM) of water. Full details of the calculated frequencies and the vibrational mode assignments are contained in the Supporting Information. The unscaled frequencies were used to calculate the $^{97}\text{Mo}/^{95}\text{Mo}$ isotope fractionation factors.

The vibrational partition functions can be used to determine the equilibrium isotope fractionation factors between two species, as the energy difference between isotopomers is due to the differences in the vibrational frequencies (the correction due to the contribution of rotational transitions is small compared to the effect of the vibrational transitions, though it can become significant at low temperatures).^{24–26} The equilibrium isotope fractionation factor for isotopes a and b between species k and l is determined from the calculated frequencies by the following method:

$${}^a Q_{\text{vib}} = \prod_i \frac{e^{-h\nu_i/2kT}}{(1 - e^{-h\nu_i/2kT})} \quad (1)$$

where ${}^a Q_{\text{vib}}$ is the vibrational partition function for the isotopomer containing a , and ν_i is an individual vibrational frequency. The partition function ratio for k is

$${}^{a-b} \beta_k = [{}^a Q_{\text{vib}} / {}^b Q_{\text{vib}}] \quad (2)$$

which is used in the form of the reduced partition function ratio. In practice, the reduced partition function ratio was calculated using

$$\ln[{}^{a-b} \beta_k] = \ln[{}^a Q_{\text{vib}} / {}^b Q_{\text{vib}}] - \ln\left[\prod_i ({}^b \nu_i / {}^a \nu_i)\right] \quad (3)$$

which approaches zero at the high-temperature limit. Here,

$$\ln\left[\prod_i ({}^b \nu_i / {}^a \nu_i)\right] = \ln[(m_a/m_b)^{3/2} (M_b/M_a)^{3/2}] \quad (4)$$

where m_a and m_b are atomic masses of isotopes a and b , and M_a and M_b are the molecular masses for isotopomers a and b . The isotopic exchange equilibrium constant is given by

$$\ln[\alpha_{k-l}] = \ln[{}^{a-b} \beta_k] - \ln[{}^{a-b} \beta_l] \quad (5)$$

and the isotope fractionation factor between k and l is expressed as

$$\Delta_{k-l} \approx 1000 \ln[\alpha_{k-l}] \quad (6)$$

The isotope fraction factor measured for a single sample relative to a reference standard is denoted $\delta^{ab}\text{Mo}_k$, and the difference between two species or samples can be expressed as

$$\Delta^{ab}\text{Mo}_{k-l} = \delta^{ab}\text{Mo}_k - \delta^{ab}\text{Mo}_l \quad (7)$$

Results and Discussion

Calculated geometries for the species under consideration have been reported previously.¹⁰ Unscaled frequencies were used in the isotope fractionation calculations because our previous work showed that the scale factor for B3LYP DFT calculations on Mo complexes was close to unity.¹⁰

TABLE 1: Mo Isotope Fraction Factors vs MoO_4^{2-} at 25 °C for Candidate Molybdic Acid Structures, Calculated in the Gas Phase via DFT with the B3LYP Functional

complex	$\Delta^{97/95}\text{Mo}_{\text{MoA-MoO}_4^{2-}}$ (‰)
MoO_3	-2.20
$\text{MoO}_3(\text{H}_2\text{O})$	-0.57
$\text{MoO}_3(\text{H}_2\text{O})_2$	-1.00
$\text{MoO}_3(\text{H}_2\text{O})_3$	-1.33
$\text{MoO}_2(\text{OH})_2$	+0.18
$\text{MoO}_2(\text{OH})_2(\text{H}_2\text{O})$	-0.53
$\text{MoO}_2(\text{OH})_2(\text{H}_2\text{O})_2$	-1.01
$\text{MoO}(\text{OH})_4$	-0.39
$\text{MoO}(\text{OH})_4(\text{H}_2\text{O})$	-1.14
$\text{Mo}(\text{OH})_6$	-0.55

Though the Raman study indicated that the structure of molybdic acid was probably $\text{MoO}_3(\text{H}_2\text{O})_3$,¹⁰ we calculated the equilibrium isotope fractionation factors between all possible structural isomers of H_2MoO_4 , including structures which corresponded to the addition or loss of one or two H_2O molecules, and MoO_4^{2-} (Table 1). For structures with the same number of oxo groups, ${}^{97}\text{Mo}/{}^{95}\text{Mo}$ $\Delta_{\text{molybdic acid-molybdate}}$ ($\Delta^{97/95}\text{Mo}_{\text{MoA-MoO}_4^{2-}}$) became more negative as additional aqua ligands were added, with the exception of MoO_3 .

MoO_3 is exceptional because it has a trigonal pyramidal structure and a low frequency (266 cm^{-1}) pyramidalization mode with a large Mo displacement. This accounts for the strong predicted concentration of the lighter isotope. The computed $\Delta^{97/95}\text{Mo}_{\text{MoA-MoO}_4^{2-}}$, -2.20 ‰, is closest to the experimental value (-1.8 ‰) of any of the species. However, MoO_3 cannot be the predominant form of molybdic acid in solution. The computed $\text{Mo}=\text{O}$ stretching frequencies are much too high to match the experimental Raman spectrum,¹⁰ and dilatometric studies²⁷ reveal an increase in coordination number when two protons are added to MoO_4^{2-} . Furthermore, the X-ray absorption spectroscopy (XAS) of Mo adsorbed to ferromanganese nodules indicates that the Mo is 6-coordinate.²⁸ $\text{MoO}_3(\text{H}_2\text{O})_3$, with $\Delta^{97/95}\text{Mo}_{\text{MoA-MoO}_4^{2-}} = -1.33$ ‰, was the next closest to the experimental data and is also favored over $\text{MoO}(\text{OH})_4(\text{H}_2\text{O})$ and $\text{MoO}_2(\text{OH})_2(\text{H}_2\text{O})_2$ as the structure of molybdic acid on the basis of Raman spectroscopy.¹⁰ How might the discrepancy between the experimental value and $\Delta^{97/95}\text{Mo}_{\text{MoA-MoO}_4^{2-}}$ for $\text{MoO}_3(\text{H}_2\text{O})_3$ be understood?

The most likely explanation is that the calculations are in the gas phase while the isotope fractionation occurs between MoO_4^{2-} in aqueous solution and molybdic acid adsorbed at an oxyhydroxide surface. Interactions with water molecules or with surface ions could alter vibrational frequencies and mode compositions.

There are two parameters for each vibrational mode that affect the partition function ratio, ${}^{97-95}\beta$: the frequency, ν , and the isotope sensitivity demonstrated by the frequency ratio, ${}^{95}\nu/{}^{97}\nu$. If ${}^{95}\nu$ increases (with ${}^{95}\nu/{}^{97}\nu$ staying the same), then $\ln[{}^{97-95}\beta]$ will increase. Since $\ln[\alpha_{\text{molybdic acid-molybdate}}] = \ln[{}^{97-95}\beta_{\text{molybdic acid}}] - \ln[{}^{97-95}\beta_{\text{molybdate}}]$, an increase in ν for a molybdic acid mode would cause $\Delta^{97/95}\text{Mo}_{\text{MoA-MoO}_4^{2-}}$ to shift in the positive direction. If ${}^{95}\nu/{}^{97}\nu$ increases (with ${}^{95}\nu$ staying the same), then $\ln[{}^{97-95}\beta]$ will increase. Thus, an increase in ${}^{95}\nu/{}^{97}\nu$ for a molybdic acid mode would also cause $\Delta^{97/95}\text{Mo}_{\text{MoA-MoO}_4^{2-}}$ to shift in the positive direction.

To model the effect of solvent we carried out PCM calculations, in which the complex sits in a cavity of appropriate size and shape in a polarizable continuous dielectric medium.^{21–23} The result was to worsen the discrepancy with experiment (Table 2). The predicted fractionation factors became less negative for

TABLE 2: Mo Isotope Fraction Factors vs MoO_4^{2-} at 25 °C from B3LYP Calculations in the Gas Phase and with a PCM Solvent Model of Water

complex	$\Delta^{97/95}\text{Mo}_{\text{MoA-MoO}_4^{2-}}$ (‰) gas phase	$\Delta^{97/95}\text{Mo}_{\text{MoA-MoO}_4^{2-}}$ (‰) PCM
MoO_3	-2.20	-4.15
$\text{MoO}_3(\text{H}_2\text{O})_3$	-1.33	-0.33
$\text{MoO}_2(\text{OH})_2(\text{H}_2\text{O})_2$	-1.01	-0.44

TABLE 3: B3LYP Calculated Frequencies, Frequency Ratios, and Mode Assignments for the ^{95}Mo and ^{97}Mo Isotopomers of MoO_4^{2-}

experimental (cm^{-1}) ^a	gas phase		PCM solvent model		assignment
	$^{95}\nu$ (cm^{-1})	$^{95}\nu/^{97}\nu$	$^{95}\nu$ (cm^{-1})	$^{95}\nu/^{97}\nu$	
317	298	1	320	1	$E \delta_s\text{MoO}$
325	314	1.00189	287	1.00139	$T_2 \delta_{\text{as}}\text{MoO}$
837	826	1.00229	777	1.00243	$T_2 \nu_{\text{as}}\text{MoO}$
897	868	1	890	1	$A_1 \nu_s\text{MoO}$

^a Experimental data for MoO_4^{2-} from ref 30.

TABLE 4: B3LYP Calculated Frequencies, Frequency Ratios, and Mode Assignments for the ^{95}Mo and ^{97}Mo Isotopomers of MoO_3

gas phase		PCM solvent model		assignment
$^{95}\nu$ (cm^{-1})	$^{95}\nu/^{97}\nu$	$^{95}\nu$ (cm^{-1})	$^{95}\nu/^{97}\nu$	
266	1.00281	321	1.00123	$\delta_s\text{MoO}$
336	1.00093	343	1.00060	$\delta_{\text{as}}\text{MoO}$
338	1.00093	343	1.00060	$\delta_{\text{as}}\text{MoO}$
963	1.00205	881	1.00191	$\nu_{\text{as}}\text{MoO}$
964	1.00205	881	1.00191	$\nu_{\text{as}}\text{MoO}$
995	1.00061	959	1.00067	$\nu_s\text{MoO}$

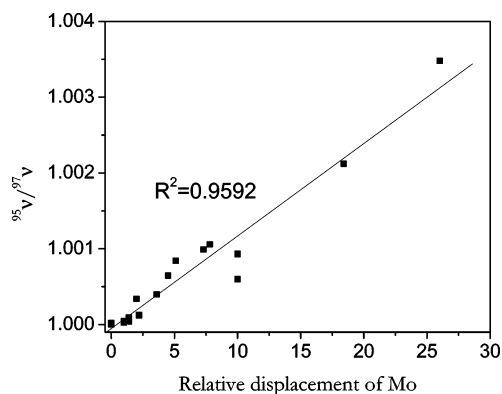
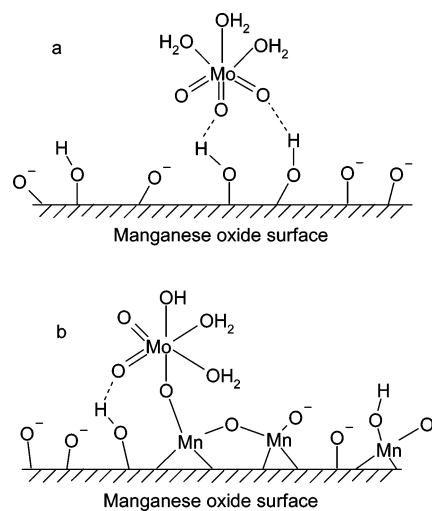
TABLE 5: B3LYP Calculated Frequencies, Frequency Ratios, and Mode Assignments for Selected Modes of the ^{95}Mo and ^{97}Mo Isotopomers of $\text{MoO}_3(\text{H}_2\text{O})_3$

gas phase		PCM solvent model		assignment
$^{95}\nu$ (cm^{-1})	$^{95}\nu/^{97}\nu$	$^{95}\nu$ (cm^{-1})	$^{95}\nu/^{97}\nu$	
123	1.00084	163	1.00179	$\delta\text{MoO}(\text{aqua})$
141	1.00106	182	1.00149	δMoO
143	1.00099	195	1.00046	δMoO
330	1.00093	346	1.00085	$\delta_{\text{as}}\text{MoO}(\text{oxo})$
331	1.00094	348	1.00076	$\delta_{\text{as}}\text{MoO}(\text{oxo})$
352	1.00348	376	1.00292	$\delta_s\text{MoO}(\text{oxo})$
948	1.00212	868	1.00209	$\nu_{\text{as}}\text{MoO}(\text{oxo})$
949	1.00212	869	1.00211	$\nu_{\text{as}}\text{MoO}(\text{oxo})$
964	1.00060	947	1.00065	$\nu_s\text{MoO}(\text{oxo})$

$\text{MoO}_3(\text{H}_2\text{O})_3$ and $\text{MoO}_2(\text{OH})_2(\text{H}_2\text{O})_2$; however, the factor became more negative for MoO_3 .

Examination of the source of these contrary effects provides insight into the problem. The effect of PCM on the MoO_4^{2-} part of the computation is small (Table 3); $^{95}\nu/^{97}\nu$ values change little, <0.0005. The PCM effect on MoO_3 is larger (Table 4) and is concentrated on the pyramidalization mode. For this mode, $^{95}\nu$ shifts up significantly from 266 to 321 cm^{-1} . However, the resulting increase in $\Delta^{97/95}\text{Mo}_{\text{MoA-MoO}_4^{2-}}$ is outweighed by the large decrease in $^{95}\nu/^{97}\nu$, by 0.0016. The decrease in $^{95}\nu/^{97}\nu$ reflects damping of the Mo displacement in the mode as the frequency increases, caused by an increased restoring force for $\text{Mo}=\text{O}$ bending due to the modeled solvent interactions. The Mo displacement is expected to vary directly with $^{95}\nu/^{97}\nu$, as illustrated in Figure 1, where $^{95}\nu/^{97}\nu$ is plotted against Mo displacement for all the computed modes of $\text{MoO}_3(\text{H}_2\text{O})_3$.

A similar effect of PCM might be expected for $\text{MoO}_3(\text{H}_2\text{O})_3$ (Table 5). Indeed the $\delta_s\text{MoO}(\text{oxo})$ mode, analogous to the

**Figure 1.** Plot of $^{95}\nu/^{97}\nu$ vs relative magnitude of Mo normal mode displacement, data from the gas-phase B3LYP calculations on $\text{MoO}_3(\text{H}_2\text{O})_3$.**Figure 2.** Schematic representation of possible (a) hydrogen bonding and (b) inner-sphere interactions of $\text{MoO}_3(\text{H}_2\text{O})_3$ with a manganese oxyhydroxide surface.

pyramidalization mode of MoO_3 , is predicted to shift up in frequency ($352 \rightarrow 376 \text{ cm}^{-1}$) and to have a lower $^{95}\nu/^{97}\nu$ (-0.00056), although the effect is smaller than in MoO_3 . The $\delta_{\text{as}}\text{MoO}(\text{oxo})$ modes are affected similarly. However, these decreases in $^{95}\nu/^{97}\nu$, which would have moved $\Delta^{97/95}\text{Mo}_{\text{MoA-MoO}_4^{2-}}$ in a negative direction and closer to the experimental value, are overridden by opposite trends in modes associated with the water ligands (see especially $\delta\text{MoO}(\text{aqua})$).

It seems likely that PCM is an inadequate model for solvation in an aqueous medium. Hydrogen bonds to and from solvent water are directional and are likely to have more specific effects on vibrations than PCM allows, especially for coordinated water molecules. Interestingly, in the calculations on MoO_4^{2-} , for which experimental data is available, the gas-phase calculations (average error = 18 cm^{-1}) were more accurate overall than the PCM calculation (average error = 27 cm^{-1}). We note that PCM did not improve agreement between theory and experiment in the calculation of the isotope fractionation between $[\text{Fe}(\text{H}_2\text{O})_6]^{3+}$ and $[\text{Fe}(\text{H}_2\text{O})_6]^{2+}$ complexes.²⁹

Another consideration is that the modeled vibrational modes should take into account interactions of the molybdic acid with the oxide surface. Figure 2 illustrates some possible modes of interaction for $\text{MoO}_3(\text{H}_2\text{O})_3$, which include outer sphere hydrogen bonding with surface hydroxyl groups and inner sphere coordination with lattice Mn^{4+} ions (bridging oxides). All these interactions should specifically increase the force constants for

TABLE 6: Comparison of Calculated Frequencies and Frequency Ratios for Selected Modes^a of MoO₄²⁻ and MoO₃

mode	level of theory					
	B3LYP ^b		B3LYP ^c		CCSD ^c	
	⁹⁵ ν	⁹⁵ ν/ ⁹⁷ ν	⁹² ν	⁹⁵ ν/ ⁹⁷ ν ^d	⁹² ν	⁹⁵ ν/ ⁹⁷ ν ^d
MoO ₄ ²⁻ δ _{as} MoO	314	1.00189	310.3	1.0020	325.5	1.0019
MoO ₄ ²⁻ ν _{as} MoO	826	1.00229	816.9	1.0023	831.8	1.0023
MoO ₃ ν _{as} MoO	963	1.00205	956.1	1.0021	947.6	1.0021

^a The symmetric stretching and bending modes of MoO₄²⁻ are not Mo isotope sensitive. ^b This work. ^c Data from ref 9. ^d In ref 9 the ratios reported are for ⁹²ν/¹⁰⁰ν which, for ease of comparison, have been converted to ⁹⁵ν/⁹⁷ν ratios here by dividing (ⁱν/^jν - 1) by four.

Mo=O and/or Mo-OH₂ bending and damp the motion of the Mo atom. A decrease in the Mo displacement would decrease ⁹⁵ν/⁹⁷ν for molybdc acid modes and cause Δ^{97/95}Mo_{MoA-MoO₄²⁻ to become more negative. Although modeling of these directional forces is beyond the scope of this study, it seems reasonable that they would increase the magnitude of the computed Δ^{97/95}Mo_{MoA-MoO₄²⁻ for MoO₃(H₂O)₃, improving the agreement between theory and experiment.}}

The effect of directional interactions in the condensed phase on vibrational frequencies and isotope fractionation factors has been quantified in a study on the isotope fractionation between [Fe(H₂O)₆]³⁺ and [Fe(H₂O)₆]²⁺ complexes.²⁹ There was 2.4 ‰ difference between Δ^{56/54}Fe_{[Fe(H₂O)₆]^{3+/2+}} derived from in vacuo DFT calculations and Δ^{56/54}Fe_{[Fe(H₂O)₆]^{3+/2+}} derived from experimental vibrational frequencies of [Fe(H₂O)₆]³⁺ and [Fe(H₂O)₆]²⁺ in crystals. (The Δ^{56/54}Fe_{[Fe(H₂O)₆]^{3+/2+}} value from the in vacuo calculation agreed with the experimental data from solution). Most of the difference was attributed to frequency changes caused by directional interactions in the crystals.²⁹ This shows that the interactions of molybdc acid with the surface can account for the discrepancy between our calculated Δ^{97/95}Mo_{MoA-MoO₄²⁻} for MoO₃(H₂O)₃ and the experimental data without major changes in the structure. The 0.47 ‰ discrepancy in the Mo system between the DFT-calculated Δ^{97/95}Mo_{MoA-MoO₄²⁻} for MoO₃(H₂O)₃ and the experimental data is smaller than the difference seen in the [Fe(H₂O)₆]^{3+/2+} system due to the heavier mass of Mo and because a surface-sorbed species can form fewer directional interactions than a species in a three-dimensional crystal lattice. It should be noted that the XAS study of Mo adsorbed to ferromanganese nodules indicated not only that it had octahedral coordination geometry but also that there were three short Mo-O bonds,²⁸ similar to the molybdc acid solution structure, MoO₃(H₂O)₃.

The isotope fractionation factors we have calculated are significantly different from those previously reported by Tossell,⁹ who found Δ^{97/95}Mo_{MoA-MoO₄²⁻} = 0.0 ‰ (B3LYP) for MoO₃(H₂O)₃ and Δ^{97/95}Mo_{MoA-MoO₄²⁻} = -1.0 ‰ (B3LYP) or -1.6 ‰ (CCSD) for MoO₃. It is difficult to determine the reasons for the differences between the results of this work and those previously reported by Tossell, as calculated frequencies and Mo isotope sensitivities were only reported for MoO₄²⁻ and the MoO₃ asymmetric stretching mode, and they do not differ greatly from the results in this work (Table 6). However, we are confident in our results, as the theoretical method chosen was validated by comparison to the experimentally determined frequencies of a variety of Mo-oxo compounds,¹⁰ and the MoO₃(H₂O)₃ structure is consistent with the Raman¹⁰ and dilatometric²⁷ data on molybdc acid in solution.

Conclusions

The species most consistent with the observed isotope fractionation of Mo between oxidic sediments and seawater and the Raman data¹⁰ on the structure of molybdc acid is MoO₃(H₂O)₃. The discrepancy between our calculated value of Δ^{97/95}Mo_{MoA-MoO₄²⁻} = -1.33 ‰ for MoO₃(H₂O)₃ and the experimental value of -1.8 ‰ is probably due to the neglect of solvation and adsorption effects. The effect of the directional interactions between MoO₃(H₂O)₃ and a manganese oxyhydroxide surface on the MoO₃(H₂O)₃ vibrations can account for this difference.

Acknowledgment. We thank Dr Andrzej Jarzecki for helpful discussions. This work was supported by the NSF through Grant OCE-0526495/0526618 to A.D.A., L.E.W., and T.G.S., and by the Center for Environmental Bioinorganic Chemistry funded by NSF Grant CHE-0221978.

Supporting Information Available: Tables containing ⁹⁵ν, the ⁹⁵ν/⁹⁷ν ratio, and the mode assignments for the gas phase and PCM calculations on Mo(OH)₄, MoO(OH)₄(H₂O), MoO₂(OH)₂, MoO₂(OH)₂(H₂O), MoO₂(OH)₂(H₂O)₂, MoO₃(H₂O), MoO₃(H₂O)₂, MoO₃(H₂O)₃, and Mo(OH)₆. This material is available free of charge via the Internet at <http://pubs.acs.org>.

References and Notes

- (1) Takematsu, N.; Sato, Y.; Okabe, S.; Nakayama, E. *Geochim. Cosmochim. Acta* **1985**, *49*, 2395-2399.
- (2) Bertine, K. K.; Turekian, K. K. *Geochim. Cosmochim. Acta* **1973**, *37*, 1415-1434.
- (3) Berran, P. G.; Grill, E. V. *Mar. Chem.* **1974**, *2*, 125-148.
- (4) Barling, J.; Arnold, G. L.; Anbar, A. D. *Earth Planet. Sci. Lett.* **2001**, *193*, 447-457.
- (5) Siebert, C.; Nägler, T. F.; von Blanckenburg, F.; Kramers, J. D. *Earth Planet. Sci. Lett.* **2003**, *211*, 159-171.
- (6) Malinovsky, D.; Hammarlund, D.; Ilyashuk, B.; Martinsson, O.; Gelting, J. *Chem. Geol.* **2007**, *236*, 181-198.
- (7) Barling, J.; Anbar, A. D. *Earth Planet. Sci. Lett.* **2004**, *217*, 315-329.
- (8) Arnold, G. L.; Anbar, A. D.; Barling, J.; Lyons, T. W. *Science* **2004**, *304*, 87-90.
- (9) Tossell, J. A. *Geochim. Cosmochim. Acta* **2005**, *69*, 2981-2993.
- (10) Oyerinde, O. F.; Weeks, C. L.; Anbar, A. D.; Spiro, T. G. *Inorg. Chim. Acta*, in press, doi: 10.1016/j.ica.2007.06.025.
- (11) Frisch, M. J.; Trucks, G. W.; Schlegel, H. B.; Scuseria, G. E.; Robb, M. A.; Cheeseman, J. R.; Montgomery, J. A., Jr.; Vreven, T.; Kudin, K. N.; Burant, J. C.; Millam, J. M.; Iyengar, S. S.; Tomasi, J.; Barone, V.; Mennucci, B.; Cossi, M.; Scalmani, G.; Rega, N.; Petersson, G. A.; Nakatsuji, H.; Hada, M.; Ehara, M.; Toyota, K.; Fukuda, R.; Hasegawa, J.; Ishida, M.; Nakajima, T.; Honda, Y.; Kitao, O.; Nakai, H.; Klene, M.; Li, X.; Knox, J. E.; Hratchian, H. P.; Cross, J. B.; Adamo, C.; Jaramillo, J.; Gomperts, R.; Stratmann, R. E.; Yazyev, O.; Austin, A. J.; Cammi, R.; Pomelli, C.; Ochterski, J. W.; Ayala, P. Y.; Morokuma, K.; Voth, G. A.; Salvador, P.; Dannenberg, J. J.; Zakrzewski, V. G.; Dapprich, S.; Daniels, A. D.; Strain, M. C.; Farkas, O.; Malick, D. K.; Rabuck, A. D.; Raghavachari, K.; Foresman, J. B.; Ortiz, J. V.; Cui, Q.; Baboul, A. G.; Clifford, S.; Cioslowski, J.; Stefanov, B. B.; Liu, G.; Liashenko, A.; Piskorz, P.; Komaromi, I.; Martin, R. L.; Fox, D. J.; Keith, T.; Al-Laham, M. A.; Peng, C. Y.; Nanayakkara, A.; Challacombe, M.; Gill, P. M. W.; Johnson, B.; Chen, W.; Wong, M. W.; Gonzalez, C.; Pople, J. A. *Gaussian 03*, rev. B.05; Gaussian, Inc.: Pittsburgh, PA, 2003.
- (12) Anbar, A. D.; Jarzecki, A. A.; Spiro, T. G. *Geochim. Cosmochim. Acta* **2005**, *69*, 825-837.
- (13) Lee, C.; Yang, W.; Parr, R. G. *Phys. Rev. B* **1988**, *37*, 785-789.
- (14) Miehlisch, B.; Savin, A.; Stoll, H.; Preuss, H. *Chem. Phys. Lett.* **1989**, *157*, 200-206.
- (15) Hay, P. J.; Wadt, W. R. *J. Chem. Phys.* **1985**, *82*, 299-310.
- (16) Ditchfield, R.; Hehre, W. J.; Pople, J. A. *J. Chem. Phys.* **1971**, *54*, 724-728.
- (17) Francl, M. M.; Pietro, W. J.; Hehre, W. J.; Brinkley, J. S.; Gordon, M. S.; DeFrees, D. J.; Pople, J. A. *J. Chem. Phys.* **1982**, *77*, 3654-3665.
- (18) Krishnan, R.; Binkley, J. S.; Seeger, R.; Pople, J. A. *J. Chem. Phys.* **1980**, *72*, 650-654.

- (19) Frisch, M. J.; Pople, J. A.; Brinkley, J. S. *J. Chem. Phys.* **1984**, *80*, 3265–3269.
- (20) Clark, T.; Chandrasekhar, J.; Spitznagel, G. W.; von Rague Schleyer, P. J. *Comput. Chem.* **1983**, *4*, 294–301.
- (21) Miertus, S.; Scrocco, E.; Tomasi, J. *Chem. Phys.* **1981**, *55*, 117–129.
- (22) Tomasi, J.; Persico, M. *Chem. Rev.* **1994**, *94*, 2027–2094.
- (23) Mennucci, B.; Tomasi, J. *J. Chem. Phys.* **1997**, *106*, 5151–5158.
- (24) Urey, H. C.; Rittenberg, D. *J. Chem. Phys.* **1933**, *1*, 137–143.
- (25) Bigeleisen, J.; Mayer, M. G. *J. Chem. Phys.* **1947**, *15*, 261–267.
- (26) Urey, H. C. *J. Chem. Soc.* **1947**, 562–581.
- (27) Cruywagen, J. J.; Rohwer, E. F. C. H. *Inorg. Chem.* **1975**, *14*, 3136–3137.
- (28) Kuhn, T.; Bostick, B. C.; Koschinsky, A.; Halbach, P.; Fendorf, S. *Chem. Geol.* **2003**, *199*, 29–43.
- (29) Jarzecki, A. A.; Anbar, A. D.; Spiro, T. G. *J. Phys. Chem. A* **2004**, *108*, 2726–2732.
- (30) Weinstock, N.; Schulze, H.; Mueller, A. *J. Chem. Phys.* **1973**, *69*, 5063–5067.